Hindawi
International Journal of Chemical Engineering
Volume 2019, Article ID 2716423, 13 pages
https://doi.org/10.1155/2019/2716423

*Research Article*

# Biosynthesis and Characterization of Iron Nanoparticles for Effective Adsorption of Cr(VI)

**Emel Simla Önal, Tolga Yatkın, Tural Aslanov, Memduha Ergüt, and Ayla Özer**

*Department of Chemical Engineering, Faculty of Engineering, Mersin University, Mersin 33343, Turkey*

Correspondence should be addressed to Memduha Ergüt; memduha.ergut@gmail.com

Received 30 November 2018; Revised 27 February 2019; Accepted 17 March 2019; Published 2 May 2019

Academic Editor: Gianluca Di Profio



In this study, iron nanoparticles (FeNPs) were synthesized via a green method using loquat *(Eriobotrya japonica)* leaves aqueous extract as a renewable reducing agent. The synthesized FeNPs were characterized by DLS, XRD, FT-IR, SEM/EDX, and TEM analysis, and then, they were used as an adsorbent for Cr(VI) removal from aqueous solutions. Batch adsorption experiments were carried out to investigate the optimum adsorption parameters such as the initial pH of the solution, temperature, initial Cr(VI) concentration, and adsorbent concentration. The optimum adsorption conditions were determined as initial pH 3.0, temperature 45°C, and adsorbent concentration 1 g/L. Also, a linear increase was observed in adsorbed Cr(VI) amounts with the increasing initial Cr(VI) concentrations. The biosynthesized FeNPs showed the high removal levels higher than 90% for Cr(VI) adsorption at a wide range of initial Cr(VI) concentrations (50–500 mg/L). The experimental equilibrium data were modelled with Langmuir and Freundlich isotherm models, and it was found that experimental equilibrium data could be well described by the Langmuir isotherm model. The maximum monolayer coverage capacity of FeNPs for Cr(VI) adsorption was found to be 312.5 mg/g. The pseudo-first-order and the pseudo-second-order kinetic models were applied to the experimental adsorption data, and it was concluded that the data were defined as the best agreement with the pseudo-second-order kinetic model. Weber–Morris model was used to investigate the effect of mass transfer on the adsorption of Cr(VI) onto FeNPs; it was observed that both the film (boundary layer) and intraparticle diffusion affected the studied adsorption process. The thermodynamic studies suggested that Cr(VI) adsorption onto FeNPs was endothermic and nonspontaneous, and the positive $\Delta S$ value indicated increased disorder at the solid-solution interface during the adsorption.

## 1. Introduction

Water pollution is one of the most important burning environmental issues among the various kinds of environmental pollution since water resources are contaminated by a variety of organic, inorganic, and biological pollutants due to day-to-day utilization and potential applications of water at domestic, industrial, and agricultural areas all over the world [1, 2].

The heavy metals (arsenic, zinc, copper, nickel, mercury, cadmium, lead, and chromium) are the best known non-biodegradable water pollutants which are extremely toxic and dangerous for the ecosystem, agriculture, and human health [3].

The chromium ions exist in industrial wastewaters both trivalent and hexavalent forms. Cr(VI) ion exists in different forms in solutions as $Cr_2O_7^{2-}$, $HCrO4^-$, or $CrO_4^{2-}$ depending on the pH and the Cr(VI) concentration. Otherwise, Cr(III) ion is relatively less toxic than Cr(VI) ion. The Cr(III) species in aqueous solutions is present in the forms of $Cr^{3+}$, $Cr(OH)^{2+}$, $Cr(OH)^{2+}$, $Cr(OH)_3$, or $Cr(OH)^{4-}$ depending on the solution pH [4, 5].

Cr(VI) is widely used in paints and pigments, chrome chemicals, leather tanning, electroplating industries, cement, and photography industries that lead to production of great quantities of effluents containing the toxic Cr(VI) ions [6]. Moreover, Cr(VI) is classified as the top 16th hazardous substance by the Agency for Toxic Diseases Registry (ATSDR) due to its carcinogenic properties and toxicity degree [4]. It is quite harmful to the living organisms because it has the potential to pass through cell membranes and reduces to reactive intermediates. These reactive

intermediates can attack DNA, proteins, and membrane lipids, and they cause damage to the cellular functions [7]. The acceptable discharge level for the hexavalent chromium ion in industrial wastewaters is reported as 0.1 mg/L by the United States Environmental Protection Agency (US EPA), and the permitted Cr(VI) ion limit in drinking water is 50 μg/L according to the World Health Organization (WHO) data [4, 5]. Therefore, to reduce Cr(VI) ion to the standard level, effective, eco-friendly and economic treatment methods should be improved.

There are commonly used treatment methods for discharging chromium ions from wastewaters such as adsorption, biosorption, coagulation, chemical precipitation, reverse osmosis, ion exchange, extraction, and membrane filtration techniques. Among them, adsorption offers a good opportunity for the removal of the chromium ion from wastewaters because of its low cost, simple operation, the capability of the trace level pollutant removal, and high efficiency [4, 6].

Recently, the usage of metal/metal oxide nanoparticles such as zero-valent iron, $Fe_3O_4$, $TiO_2$, ZnO, and their composites as a sorbent has attracted great attention in the treatment of various heavy metals like chromium. The advantage of these functional nanomaterials is high adsorption capacity that is associated with their large specific surface area and high reactivity in the adsorption processes [3].

Biosynthetic approaches are quite popular for the synthesis of metal nanoparticles using microorganisms, enzyme, and plant extracts, due to their predominant advantages compared to traditional chemical synthesis methods including toxic and expensive compounds such as $NaBH_4$ as the reducing agent. Among biosynthetic procedures, the exploitation of plant extracts has a privileged position for nanoparticle preparation since plant leaves are inexpensive, natural, environmentally friendly, harmless, readily available, and suitable for scale-up steps. Loquat (*Eriobotrya japonica*) is an Asian yellow fruit belonging to the Rosaceae family, and its leaves are used widely for medicinal purpose against cough and asthma diseases in Turkey [8, 9]. Loquat leaves are very rich in terms of phenols, flavonoids, triterpene acids, and polysaccharides. These special compounds act as a bioreduction agent for metallic ions.

To the best of our knowledge, loquat leaves extract was used for the synthesis of silver and gold nanoparticles [10, 11], but this is the first study reported in literature about usage of loquat leaves aqueous extract for the green synthesis of FeNPs. However, biosynthesized zero-valent iron nanoparticles [12]; crystalline and amorphous Fe and Al-oxides such as hematite [$\alpha$-$Fe_2O_3$], goethite [$\alpha$-FeOOH], and alumina [$\alpha$-$Al_2O_3$] [4, 13]; and composite materials including iron minerals such as $Fe_3O_4$ magnetite graphene oxide encapsulated in calcium alginate beads [7] and Fe-modified activated carbon [14] were reported as effective adsorbents for removal of Cr(VI) ions.

The aim of the present study was the synthesis of iron nanoparticles (FeNPs) using *Eriobotrya japonica* leaves aqueous extract as a reducing/capping agent and investigating the Cr(VI) adsorption efficiency. For this purpose, the systematic characterization studies of synthesized FeNPs were carried out by DLS, XRD, FT-IR, SEM/EDX, and TEM analysis methods, and then, the adsorbent properties of FeNPs for Cr(VI) removal were investigated in a batch system.

## 2. Materials and Methods

*2.1. Materials.* All the chemicals used in experiments were of analytical grade, and they were used without further purification. $FeSO_4{\cdot}7H_2O$ to be used in the synthesis of FeNPs and 1,5-diphenylcarbazide were supplied from Carlo Erba and acetone (>99.5%), and HCl (37%) were provided from Sigma-Aldrich. A stock solution of 1000 mg/L of Cr(VI) was prepared by dissolving the appropriate amount of $K_2Cr_2O_7$ (Carlo Erba) in 1000 mL of distilled water. The solution with desired Cr(VI) concentration was prepared by appropriate dilutions from stock Cr(VI) solution. The pH values of the solutions were adjusted with 0.1 N hydrochloric acid and 0.1 N sodium hydroxide.

*2.2. Biosynthesis of FeNPs.* Loquat (*Eriobotrya japonica)* leaves were collected from loquat trees grown in Mersin, Turkey. Aqueous extract of *E. japonica* leaves was prepared by heating a certain amount of air-dried leaves as its concentration will be 60 g/L, at 100°C, with 500 ml of distilled water for 1 h. Subsequently, the filtered aqueous extract was added to 0.1 mol/L $FeSO_4{\cdot}7H_2O$ solution in 1 : 1 volume ratio, and the final mixture was kept under vigorous stirring for 3 h [15]. The immediate changing of the colour of the solution from clear to intense black indicated the formation of FeNPs. The formed nanoparticles were separated by evaporating water from solution on a hot plate and then collected nanoparticles, washed several times with deionized water, and dried in an oven at 120°C overnight.

*2.3. Characterization of FeNPs.* The mean hydrodynamic particle-size and size distribution of the green-synthesized FeNPs were measured by dynamic light scattering (DLS) analysis with the Malvern Zetasizer. The functional groups of FeNPs before and after adsorption were determined by Fourier transform infrared (FT-IR) spectrometer in the range of 4000–400 $cm^{-1}$. The crystal structure was observed by X-ray powder diffraction (XRD) analysis, using nickel-filtered Cu K$\alpha$ radiation in a Philips XPert MPD apparatus operated at 40 kV and 30 mA, in the $2\theta$ range of 10°–90°. The morphology of the FeNPs was analyzed by scanning electron microscope (SEM) analysis with Zeiss/Supra 55 SEM and transmission electron microscope (TEM). For the TEM study, nanoparticle samples were sonicated in analytical grade methanol and mounted on 200-mesh formware-coated copper grid and allowed to dry. TEM images were obtained using the instrument (JEOL JEM 1011 TEM) which was operated at an acceleration voltage of 80 kV, and mean diameters of particles were determined using the Image J software program.

The elemental identification and quantitative compositional information of the adsorbent were determined by Zeiss/Supra 55 energy dispersive X-ray analyzer (EDX) before and after adsorption.

The pH at the point of zero charge ($pH_{PZC}$) of prepared FeNPs was obtained by measuring the $\zeta$ (zeta) potential at different ranges of pH (2.5–12) with Zetasizer (Malvern Zetasizer Nano ZS model). The pH values of the FeNPs suspensions were adjusted from 2.5 to 12 by adding 0.1 M HCl or 0.1 M NaOH solutions as required.

*2.4. Batch Adsorption Studies.* The adsorption experiments were carried out in 250 mL Erlenmeyer flasks containing 100 mL of Cr(VI) adsorption solution. 0.1 g of FeNPs, except for adsorbent concentration experiments, was contacted with 100 mL of Cr(VI) solution at the known initial Cr(VI) concentration and initial pH. Then, the flasks were agitated at a constant temperature and shaking rate for 480 min which is more than ample time for adsorption equilibrium. Samples were taken before mixing the FeNPs, metal bearing solution, and at predetermined time intervals for determining the unadsorbed metal ion concentrations in the solution. Samples were centrifuged at 3500 rpm for 5 min, and the supernatant liquid was analyzed.

Experiments were repeated for different initial pH values (3–8), initial Cr(VI) concentration (50–500 mg/L), temperature (25–55°C), and adsorbent concentration (0.5–3 g/L) values. The adsorbed amount ($q_e$ (mg/g)) and the percentage of adsorption (adsorption (%)) at equilibrium were calculated as follows:

$$q_e\,(\mathrm{mg/g}) = \frac{C_0 - C_e}{m} \cdot V,$$
$$\text{adsorption}\,(\%) = \left[\frac{(C_0 - C_e)}{C_0}\right] \cdot 100, \tag{1}$$

where $C_0$ (mg/L) and $C_e$ (mg/L) are the initial and equilibrium concentrations of Cr(VI) solution, respectively; $m$ (g) is the mass of the adsorbent; and $V$ (L) is the volume of the liquid phase.

*2.5. Analysis Method of Cr(VI).* The unadsorbed Cr(VI) concentration was analyzed in a spectrophotometer (Cheibos UV-Vis model) according to the standard colorimetric method, using 1,5-diphenylcarbazide as the complexing agent at the wavelength of 540 nm [16].

*2.6. Error Functions.* The goodness of fit of the kinetic and isotherm equations to the experimental data was evaluated using the chi-square test and ($\chi^2$) and root-mean-square error (RMSE). An error function is defined to enable the optimization process and to evaluate the fit of the isotherm equation to the experimental data.The chi-square test ($\chi^2$) and root-mean-square error (RMSE) values were calculated using the Microsoft Excel software by the following equations:

$$\chi^2 = \sum_{i=1}^{n} \frac{\left(q_{i,\mathrm{exp}} - q_{i,\mathrm{cal}}\right)^2}{q_{i,\mathrm{exp}}},$$
$$\mathrm{RMSE} = \sqrt{\left(\frac{1}{n}\right)\sum_{i=1}^{N}\left(q_{i,\mathrm{exp}} - q_{i,\mathrm{cal}}\right)^2}, \tag{2}$$

where $q_{i,\mathrm{cal}}$ and $q_{i,\mathrm{exp}}$ refer to the theoretical and experimental adsorption capacities (mg/g), respectively, and $n$ is the number of experimental observations.

## 3. Results and Discussion

*3.1. Characterization Studies.* The mean hydrodynamic diameter of the FeNPs was found to be approximately 171.2 nm with a polydispersity index (PDI) value of 0.217 by DLS analysis. Particle-size distribution of the green-synthesized FeNPs by DLS analysis is presented in Figure 1.

The SEM images of the synthesized FeNPs at different magnifications are presented in Figures 2(a)–2(e) before and after adsorption, respectively. SEM images revealed that FeNPs were synthesized successfully. The mean particle size of the synthesized FeNPs was determined to be 89 nm by the Image J software program. As seen from Figures 2(a)–2(c), the formed nanoparticles have irregular spherical and porous morphology which is indicating a chain structure, and nanoparticles are quite agglomerated. According to Figures 2(a)–2(c), it was seen that the agglomeration tendency of nanoparticles gave rise to the formation of nanoparticles which had higher mean hydrodynamic diameters. Therefore, the mean hydrodynamic diameters of nanoparticles were found as higher than 100 nm by DLS analysis may be due to the absorption effects and particle scattering because of agglomeration [17]. After Cr(VI) adsorption, as shown from Figures 2(d) and 2(e), it was observed that the nanoparticles were more agglomerated, and the pores were closed due to the adsorption of Cr(VI) anions onto the adsorbent surface.

In order to check the morphology and support the formation of synthesized FeNPs, TEM analysis was carried out. The obtained TEM micrograph is presented in Figure 3, and the image which was taken at higher magnification (60KX) is presented in the inset of Figure 3. According to the TEM image, it was shown that the spherical particles were obtained whose diameters were 55.4 nm, 70.31 nm, and 114.29 nm, from left to right, respectively. Moreover, it was shown from the image which was presented in the inset of Figure 3, the agglomeration behavior was observed leading to the formation of particles with bigger sizes. This result supported the SEM images.

Elemental analysis results of loquat leave extracts and FeNPs before and after adsorption are given in Table 1. According to Table 1, the elemental and quantitative weight composition (wt.%) of synthesized FeNPs were composed of 28.70% Fe, 37.53% O, 18.31% C, 12.55% S, 2.642% K, and 0.243% Mg elements. EDX analysis results revealed high Fe and O elements content and the presence of C, O, K, and Mg elements which were derived from aqueous leaves extract.

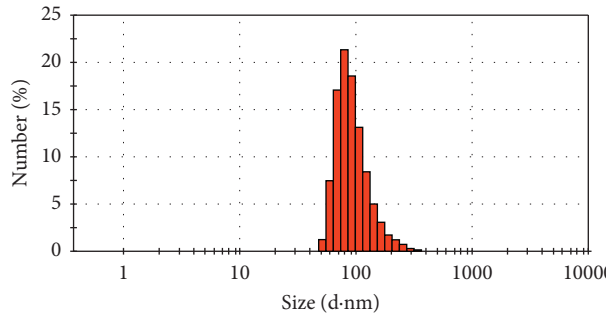


Figure 1: Particle-size distribution of FeNPs

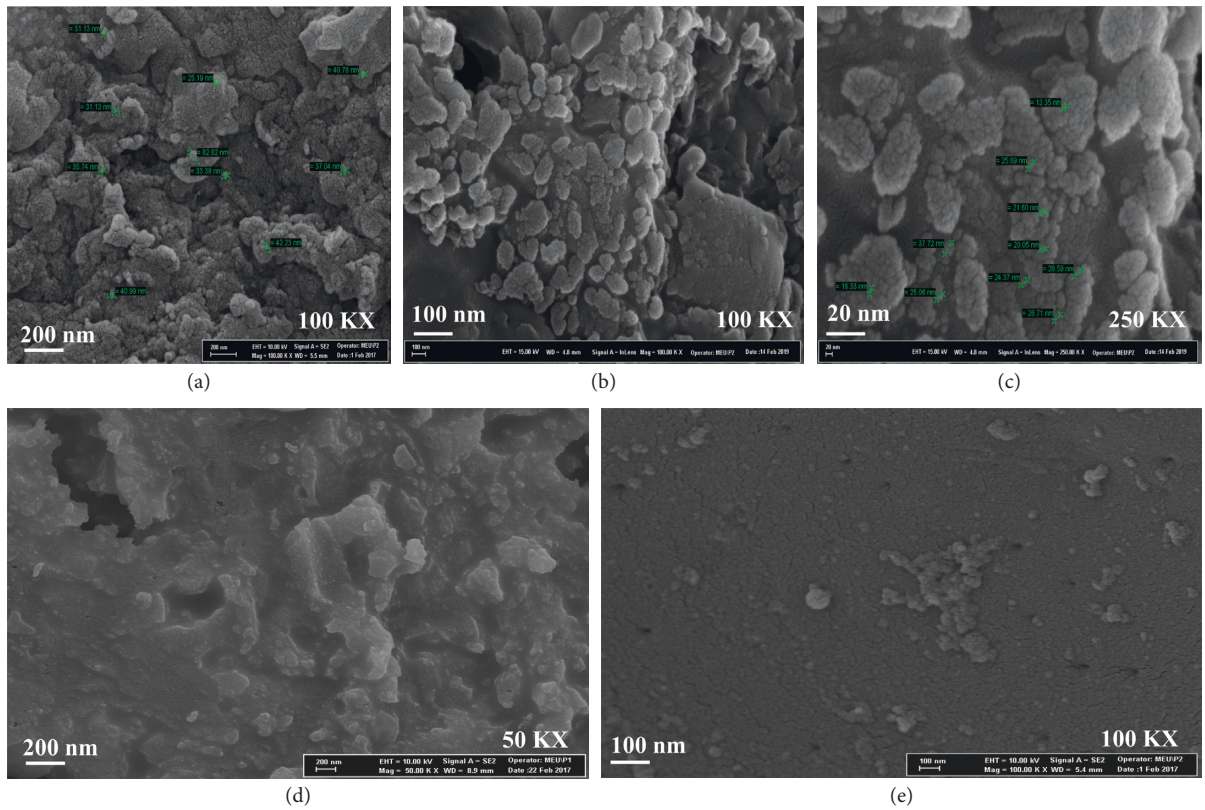


Figure 2: SEM images of FeNPs at different magnifications (a–c) before and (d, e) after adsorption.

The C signals are attributed to the polyphenol groups and other C-containing molecules [15]. Also, S element must be originating from extract and $FeSO_4 \cdot 7H_2O$ precursor used in the synthesis of FeNPs. After adsorption, the presence of the Cr element in the elemental composition confirmed the binding of the Cr(VI) ions onto the FeNPs surface.

The XRD pattern of synthesized FeNPs is given in Figure 4, where the peaks at $2\theta = 25.9^{\circ}$, $28.3^{\circ}$, and $35.6^{\circ}$ correspond to iron oxohydroxide, maghemite ($\gamma$-$Fe_2O_3$), and magnetite ($Fe_3O_4$), respectively. Also, the intensity peak at $2\theta = 17.56^{\circ}$ was identified to belong to an organic matter in polyphenols reported in the literature [15, 18]. As seen from Figure 4, the relatively weak peaks in the XRD diagram indicate that synthesized nanoparticles have amorphous grains [15]. Moreover, some studies in the literature have reported that FeNPs synthesized by the plant extract are amorphous [15, 18]. Also, after Cr(VI) adsorption, the XRD diagram of green-synthesized FeNPs indicated that the material was completely amorphous (figure not shown). The differences in the XRD patterns of FeNPs between before and after adsorption may be due to change in the crystallinity and phase of the FeNPs during the chemisorption of Cr(VI).

FT-IR study of crude extract and FeNPs before and adsorption was carried out to investigate the functional groups responsible for adsorption. The absorption bands were observed in all the samples, as presented in Figures 5, 6(a), and 6(b), respectively.

In the FT-IR spectrum of loquat leaves extract (Figure 5), the broad band at 3270.9 $cm^{-1}$ may correspond to the surface -OH group which is related to the phenolic compounds. The bands that observed at the wavenumbers of 2928 $cm^{-1}$ and

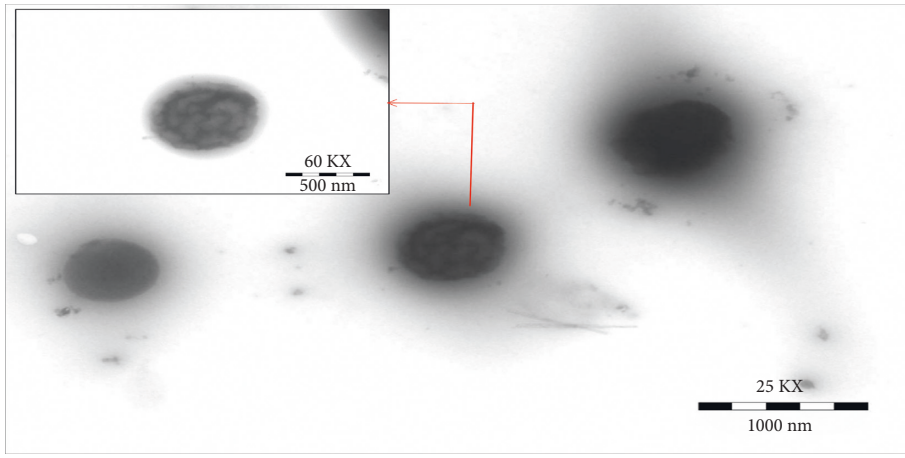


Figure 3: TEM images of synthesized FeNPs.

Table 1: Elemental analysis results for FeNPs before and after adsorption.

| Element | Weight (%) | | |
|---|---|---|---|
| | *E. japonica* leaves extract | Green-synthesized FeNPs | After Cr(VI) adsorption |
| O | 37.47 | 37.53 | 25.12 |
| Fe | – | 28.70 | 21.13 |
| C | 42.22 | 18.31 | 22.53 |
| S | 0.62 | 12.55 | 10.52 |
| K | 8.83 | 2.642 | 3.580 |
| Mg | 1.52 | 0.243 | 0.110 |
| Ca | 5.03 | — | — |
| Cl | 3.91 | — | 13.53 |
| Si | 0.37 | — | — |
| Cr | — | — | 3.435 |

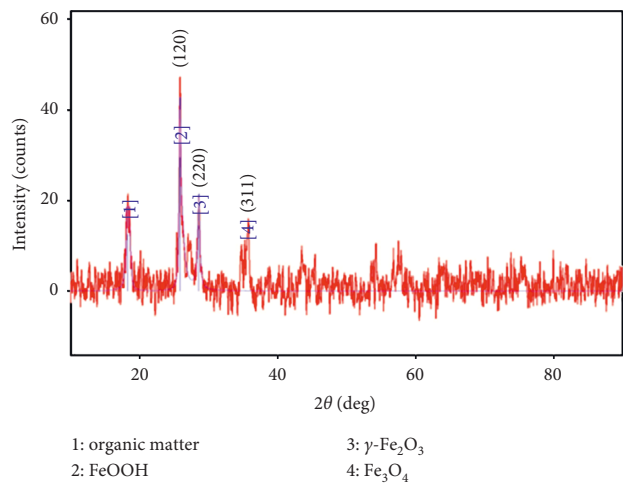


Figure 4: XRD pattern of FeNPs.

2187 $cm^{-1}$ are because of the C-H stretching vibration of the $-CH_2$ and $CH_3$ functional groups [12, 19]. The band at 1720 $cm^{-1}$ is identified as the carbonyl group from dimerized saturated aliphatic acids [20], and the bands at 1595.36 $cm^{-1}$ and 1378.12 $cm^{-1}$ are attributed to C=O, C-O stretching and the presence of C-O stretching in carboxyl groups, respectively. The broad band at 1243 $cm^{-1}$ corresponds to the C-O-C or C=O stretching vibration, and the band at 1036 $cm^{-1}$ may be assigned to C-O-C and O-H absorption [20]. Moreover, the bands observed at 889.03, 763.93, and 599.63 $cm^{-1}$ correspond to phenol groups and bending vibrations of aromatics, carboxylic acids, and amides [12]. These peaks demonstrate the presence of phenolics could be probably responsible for the bioreduction of $Fe^{2+}$ ions and formation of FeNPs.

According to the FT-IR spectrum of synthesized FeNPs (Figure 6(a)), the bands at 3236.66 $cm^{-1}$ and 2155 $cm^{-1}$ are attributed to the O-H group related to the phenolic compounds and C-H stretching vibrations of $-CH_2$ and $CH_3$ functional groups. The band at 1605 $cm^{-1}$ corresponds to C=O stretching, and the band at 1077.78 $cm^{-1}$ is due to C-O stretching [21]. Moreover, the peaks at 400 $cm^{-1}$–550 $cm^{-1}$ indicated the tetrahedral and octahedral Fe-O bonds and 596.17 $cm^{-1}$ and 458.88 $cm^{-1}$ refer to Fe-O stretches of $Fe_3O_4$ and $Fe_2O_3$ [2, 21]. After Cr(VI) adsorption, as seen from Figure 6(b), a slight change was observed in the peaks due to chemisorption of Cr(VI) ions. Based on the FT-IR results, the adsorption mechanism of the Cr(VI) ions onto FeNPs may result due to the chemical interaction between -OH and -C=O functional groups on the FeNPs surface and Cr(VI) ions in the solution [2].

### 3.2. Effects of Environmental Conditions on the Cr(VI) Adsorption onto FeNPs

*3.2.1. Effect of Initial pH.* The initial pH of the solution is an important factor in the adsorption capacity due to its impact on the ionic forms of chromium in solutions and the surface properties of the adsorbent [7]. The effect of the initial pH on the adsorption of Cr(VI) ions onto FeNPs is presented in Figure 7. According to Figure 7, Cr(VI) removal by green-synthesized FeNPs is a pH-dependent adsorption system. The maximum equilibrium uptake value was found to be 99.28 mg/g at pH 3.0 and then started to gradually decrease when the pH value was increased up to 8.0.

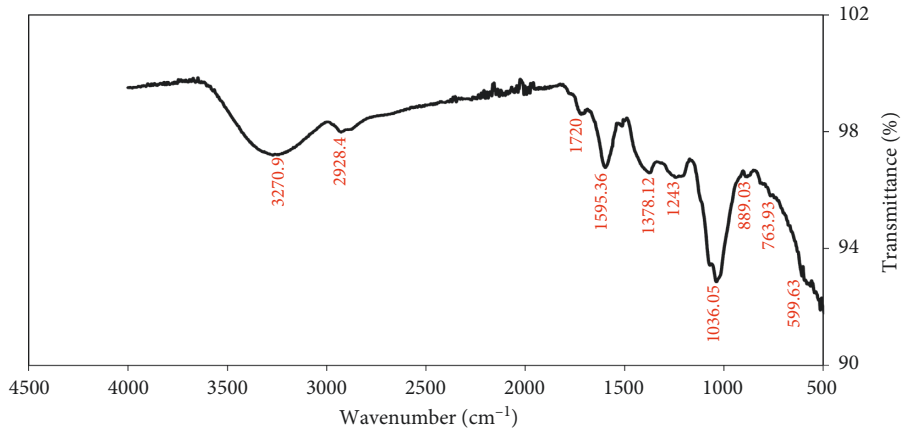


Figure 5: FT-IR spectrum of loquat (*Eriobotrya japonica)* leaves aqueous extract.

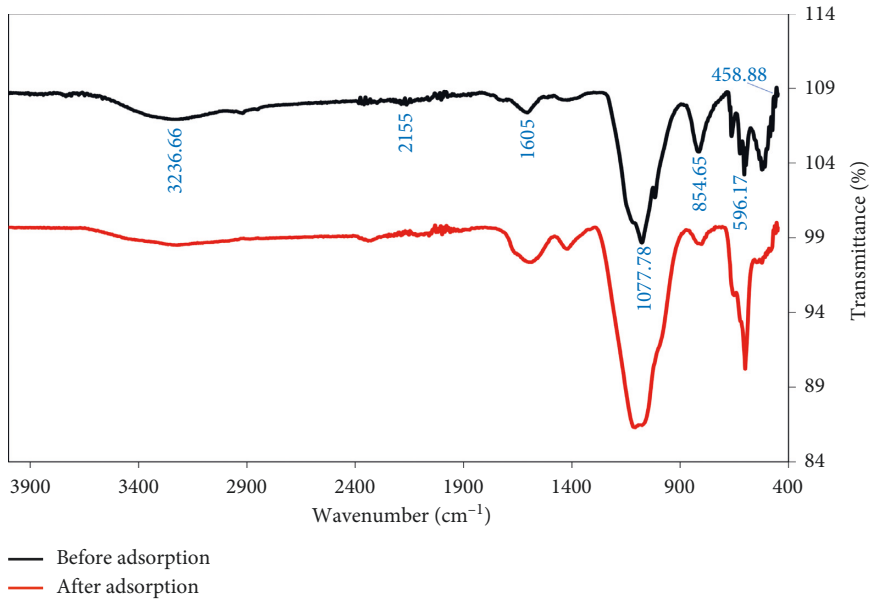


Figure 6: FT-IR spectrum of FeNPs.

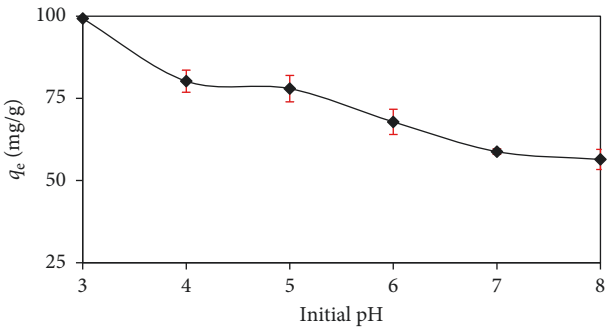


Figure 7: The effect of initial pH (initial Cr(VI) concentration 100 mg/L, adsorbent concentration 1 g/L, and temperature 25°C).

Cr(VI) ion exists in solution as $Cr_2O_7^{2-}$, $HCrO_4^-$, or $CrO_4^{2-}$, and their solubilities are strongly dependent on the solution pH and the initial Cr(VI) concentration.

The logarithmic concentration diagram for the species distribution of Cr(VI) in an aqueous system is shown in Figure 8 [4]. According to this diagram, $HCrO_4^-$ is the dominant form of Cr(VI) at the acidic medium in the range of pH 2.0–4.0; $CrO_4^{2-}$ is the predominant form in a neutral and basic medium pH 7.0 [4, 7, 22]. $HCrO_4^-$ ions occur as a result of the hydrolysis of dichromate ions, and an increase in pH would ease the formation of $Cr_2O_7^{2-}$ from $HCrO_4^-$ [23].

The formation of different species of Cr(VI) in aqueous solutions was given by the following equations:

$$\begin{aligned} Cr_2O_7^{2-} + H_2O &\longrightarrow 2HCrO_4^- \\ HCrO_4^- &\longrightarrow CrO_4^{2-} + H^+ \end{aligned} \quad (3)$$

In this study, the active form of Cr(VI) was chosen as $HCrO_4^-$ because of obtaining high removal in the acidic medium.

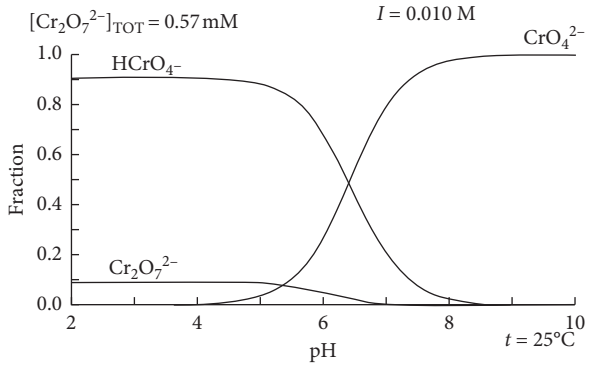


Figure 8: The concentration diagram for Cr(VI) species depends on pH.

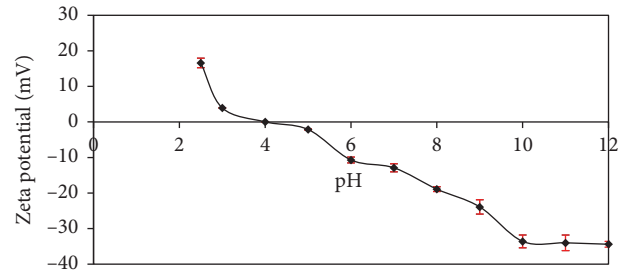


Figure 9: The isoelectric point of the prepared FeNPs.

The attitude of the maximum adsorption capacity at pH 3.0 can be explained by the isoelectric point of adsorbent. The isoelectric point of FeNPs ($pH_{pzc}$) was determined as 4.0 by the zeta ($\zeta$) potential measurement. The change of the zeta potential with pH is presented in Figure 9.

The surface of adsorbent was charged positively at the lower pH values than the isoelectric point of adsorbent and adsorption capacity increased due to strong electrostatic attraction between positively charged adsorbent surface and negatively charged $HCrO_4^-$ ions. Conversely, at the higher pH values than the isoelectric point of adsorbent, the number of negatively charged sites increased, and the number of positively charged sites decreased, so Cr(VI) adsorption capacity decreased due to the electrostatic repulsion between adsorbent surface and $HCrO_4^-$ ions.

Metal ion adsorption onto hydrous solids such as metal oxides is a complex reaction between surface sites and adsorbent. The developed surface sites for a hydrated adsorbent were formulated as follows:

$$\begin{aligned} S{-}OH_2^+ &= S{-}OH + H^+ \\ S{-}OH &= S{-}O^- + H^+ \end{aligned} \quad (4)$$

where S represents the FeNPs surface sites and $S{-}OH_2^+$, $S{-}OH$, and $S{-}O^-$ refer to protonated, neutral, and deprotonated surface hydroxyl functional groups, respectively. In this work, at the pH value below $pH_{pzc}$, the positively charged adsorbent surface ($S{-}OH^{2+}$) accelerated the uptake of the anionic $HCrO_4^-$ adsorption after which the Coulombic interaction forces can easily occur [23].

Therefore, two possible reactions would be suggested as given below in equations (5) and (6) about the adsorption mechanism depending on the interaction between $HCrO_4^-$ ions and the surface sites of adsorbent at the pH value below $pH_{pzc}$ [4]:

$$=SOH_2^+ + HCrO_4^- \Longleftrightarrow =SOH_2^+(HCrO_4^-) \quad \text{for } pH < pH_{pzc} \quad (5)$$

$$=SOH_2^+ + HCrO_4^- \Longleftrightarrow =SHCrO_4 + H_2O \quad \text{for } pH < pH_{pzc} \quad (6)$$

where $= SOH_2^+ (HCrO_4^-)$ and $= SHCrO_4$ are the bonding complexes.

*3.2.2. Effect of Initial Cr(VI) Concentration.* The initial metal ion concentration is an important factor on the adsorption capacity in terms of providing the higher driving force to overcome mass transfer resistances of the metal ions between the aqueous and solid phases. The effect of initial Cr(VI) concentration on adsorption and removal efficiency of FeNPs in the studied initial Cr(VI) concentrations was depicted in Figure 10(a) and 10(b), respectively. As seen from Figure 10(a), the adsorption capacities increased linearly when the initial concentrations of Cr(VI) were increased. By increasing the initial concentration of Cr(VI), the number of collisions with FeNPs increases which consequently enhances the rate aggregation and provides more surface binding sites available for Cr(VI) adsorption. The equation of $q_e$ versus $C_0$ was found as $q_e$ (mg/g) = 0.9453 ∗ $C_0$ (mg/L), ($R^2$ = 0.997) at optimum temperature 45°C, initial pH 3.0, 1.0 g/L adsorbent concentration, and 480 min equilibrium time for the range of the studied initial Cr(VI) concentration. According to the equation, the higher removal amounts can be obtained at higher initial Cr(VI) concentrations since the adsorption process has not shown a saturation trend in the range of 50–500 mg/L of initial Cr(VI) concentrations, yet. Also, as seen in Figure 10(b), high adsorption percentages (>90%) were obtained for Cr(VI) adsorption in the studied initial Cr(VI) concentration range.

*3.2.3. Effect of Adsorbent Concentration.* The adsorbent concentration effect on the percentage of adsorption and equilibrium uptake is presented in Figure 11. According to Figure 11, the equilibrium uptakes of FeNPs for Cr(VI) concentrations decreased with the increasing adsorbent concentration from 0.5 g/L to 3 g/L. However, the adsorption percentage increased up to 1.0 g/L of adsorbent concentration and then slightly remained constant with further increase in adsorbent concentration. The decrease in uptake values with increasing adsorbent concentration may arise from the interaction between adsorbent particles such as aggregation, resulting from high adsorbent concentration. The agglomeration of the adsorbent particles would lead to a decrease in the active surface area of the adsorbent and an

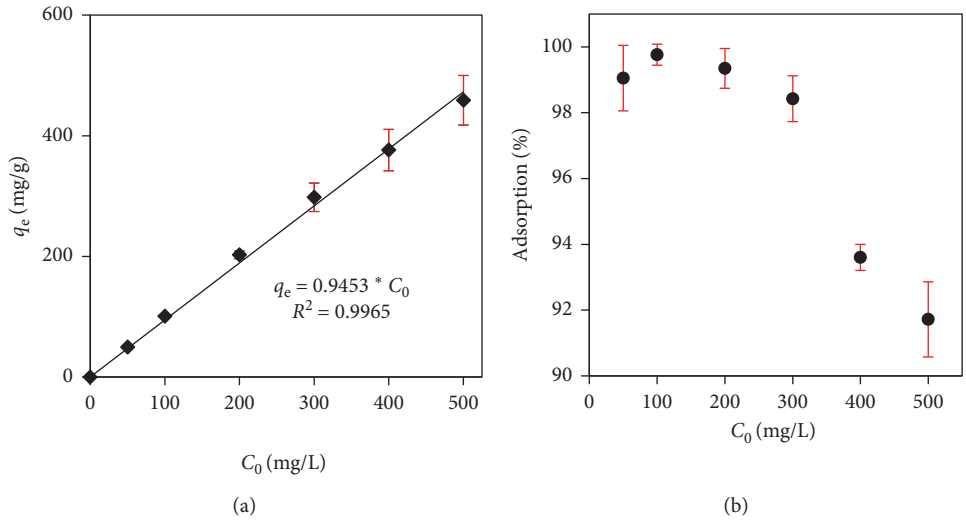


Figure 10: (a) Effect of initial Cr(VI) concentration; (b) removal efficiency of FeNPs in the studied initial Cr(VI) concentrations (temperature 45°C, initial pH 3, adsorbent concentration 1 g/L, and 480 min contact time).

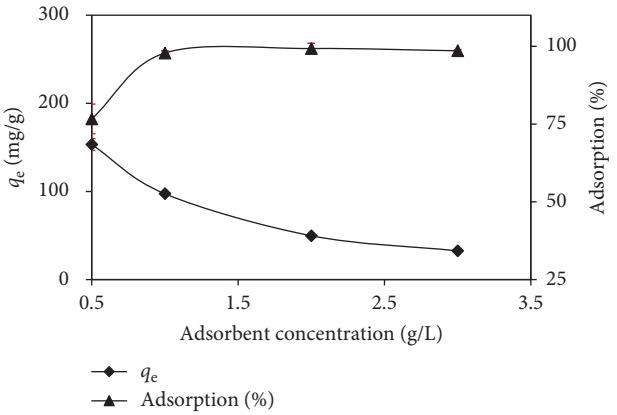


Figure 11: Effect of adsorbent concentration (temperature 45°C, initial pH 3, contact time 90 min, and initial Cr(VI) concentration 100 mg/L).

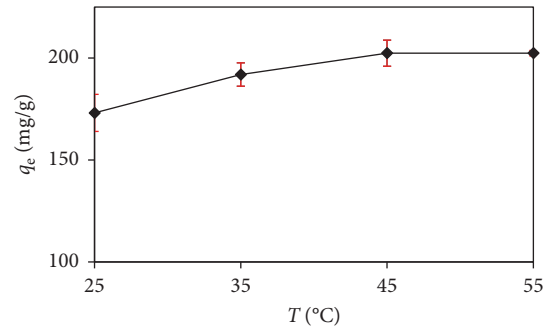


Figure 12: Effect of temperature (initial pH 3, initial Cr(VI) concentration 200 mg/L, and adsorbent concentration 1 g/L).

increase in diffusional path length. Hence, the lower adsorption capacities were observed at high adsorbent concentrations. As a result, the optimum adsorbent concentration was selected as 1.0 g/L for Cr(VI) ion adsorption onto FeNPs.

*3.2.4. Effect of Temperature.* The effect of temperature on adsorption was investigated in the range of 25–55°C temperature values. The effect of temperature on the adsorption is presented in Figure 12. According to Figure 12, it was seen that high adsorption capacity was obtained with an increase in temperature from 25°C to 45°C, and then, adsorption capacity moderately remained constant at 55°C. Therefore, the optimum temperature value for Cr(VI) adsorption was determined as 45°C. Based on the results, high operation temperature indicated that the studied adsorption process was endothermic nature.

The temperature effect on the studied adsorption process was also evaluated with thermodynamic studies by calculating the entropy change ($\Delta S$), enthalpy change ($\Delta H$), and Gibbs energy change ($\Delta G$). $\Delta G$, $\Delta H$, and $\Delta S$ were determined using the following equations [24]:

$$\ln K_c = \left(\frac{\Delta S}{R}\right) - \left(\frac{\Delta H}{R}\right) \cdot \frac{1}{T}, \tag{7}$$

$$\Delta G = -RT \ln K_c = \Delta H - T\Delta S, \tag{8}$$

where $\Delta H$ and entropy change $\Delta S$ were calculated from the slope and intercept of the linear plot of $\ln K_c$ versus $1/T$ according to the Van't Hoff equation (equation (7) while $\Delta G$ was calculated according to equation (8).

The equilibrium constant ($K_c$) values were calculated from the following equation [1]:

$$K_c = \frac{C_{ad,e}}{C_e}, \tag{9}$$

where $C_{ad,e}$ and $C_e$ are the adsorbed metal ion concentration (mg/L) and the unadsorbed metal ion concentration at equilibrium (mg/L), respectively. When the adsorbent

concentration is 1.0 g/L, $C_{ad,e}$ is equal to $q_e$ at the studied temperature.

In this study, the linear form of Van't Hoff equation for the adsorption of Cr(VI) onto FeNPs was found as $\ln K_c = -8041x(1/T) + 23.03$ with the regression coefficient 0.999 (data not shown), and the thermodynamic parameters were calculated and are presented in Table 2.

The calculated $\Delta G$ values had positive indicating that adsorption of Cr(VI) on FeNPs was nonspontaneous. The positive value of $\Delta S$ suggested randomness of the adsorbed Cr(VI) species at the solid-solution interface during adsorption [5]. Moreover, the calculated $\Delta H$ values higher than 42 kJ/mol indicated the process results from chemisorption of the Cr(VI) ions onto FeNPs [25]. Consequently, the thermodynamic parameters such as Gibb's free energy change ($\Delta G$), enthalpy change ($\Delta H$), and entropy change ($\Delta S$) supported the results of the temperature effect.

*3.3. Equilibrium, Kinetic, and Mass Transfer Modelling.* The Langmuir and Freundlich isotherm models are commonly used to describe the adsorption data and get the idea about the interactions of adsorbed materials with the adsorbent [26]. The Langmuir isotherm model suggests monolayer adsorption occurring on a homogeneous surface comes from the finite number of similar active sites, and the Freundlich isotherm model is valid for adsorption to take place on a heterogeneous surface [25]. The well-known linearized forms of Langmuir and Freundlich isotherm models are given as follows:

$$\text{Langmuir: } \frac{1}{q_e} = \frac{1}{Q^\circ b} \cdot \frac{1}{C_e} + \frac{1}{Q^\circ},$$
$$\text{Freundlich: } \ln q_e = \ln K_F + \left(\frac{1}{n}\right)\ln C_e. \tag{10}$$

The linear forms of Langmuir and Freundlich isotherm models were applied to experimental equilibrium data at different temperatures. The isotherm constants calculated from the isotherm equations with regression coefficients and error function values are summarized in Table 3.

Also, the experimental and predicted isotherms for Cr(VI) adsorption at 45°C and initial pH 3 are given in Figure 13. As seen from Table 3 and Figure 13, Langmuir isotherm model was in better agreement with experimental equilibrium data due to the high regression coefficients and lower $\chi^2$ and RMSE error function values.

This result demonstrated that the adsorption occurred at specific homogeneous sites within the adsorbent forming monolayer coverage of Cr(VI) at the surface of FeNPs. The maximum monolayer coverage capacity of adsorbent was determined as 312.5 mg/g at 45°C. As seen from Table 3, the maximum monolayer coverage capacity values of FeNPs for Cr(VI) were increased by increasing temperature may be due to the endothermic nature of the studied adsorption process.

The adsorption capacity of green-synthesized FeNPs in this study for the removal of Cr(VI) was compared with those of other adsorbents reported in the literature, and their adsorption capacities are presented in Table 4. According to Table 4, synthesized FeNPs in this study have a good adsorption capacity in comparison with most of the other adsorbents. However, the exact comparison of adsorption capacity of adsorbents is difficult due to the differences in optimum experimental conditions and physicochemical properties of adsorbents such as functional groups and specific surface areas.

Table 2: Thermodynamic parameters of the adsorption system.

| Thermodynamic parameters | | | | |
|---|---|---|---|---|
| $T$ (K) | $K_c$ | $\Delta H$ (kJ/mol) | $\Delta S$ (kJ/mol·K) | $\Delta G$ (kJ/mol) |
| 298 | 0.01905 | | | 9.813 |
| 308 | 0.04703 | 66.853 | 0.1915 | 7.828 |
| 318 | 0.10389 | | | 5.986 |

The adsorption kinetics were elucidated by correlating the adsorption kinetic data of the Cr(VI) onto FeNPs using the linear forms of the pseudo-first-order and the pseudo-second-order kinetic models [30]. The linearized forms of pseudo-first-order and the pseudo-second-order kinetic models were given in the following equations:

$$\text{pseudo-first-order: } \log(q_e - q_t) = \log(q_e) - \frac{k_1 t}{2.303}, \tag{11}$$

$$\text{pseudo-pseudo-second-order: } \frac{t}{q_t} = \left(\frac{1}{q_e^2 k_2}\right) + \frac{t}{q_e}. \tag{12}$$

For the adsorption of Cr(VI) onto FeNPs, the parameters of the pseudo-first-order and pseudo-second-order kinetic models with regression coefficients are presented in Tables 5 and 6, respectively. From Tables 5 and 6, the adsorption kinetics of Cr(VI) onto FeNPs were better described by the pseudo-second-order kinetic model due to the consistency of the experimental and calculated $q_e$ values and high regression coefficients and lower error functions than the pseudo-first-order model at all initial Cr(VI) concentrations. Based on the assumptions of the pseudo-second-order model, the chemisorption was the rate-determining step in the adsorption of Cr(VI) on FeNPs.

To evaluate the boundary layer and intraparticle diffusion mechanism between Cr(VI) ions and FeNPs, Weber–Morris model was used, and model parameters and regression coefficients are summarized in Table 7. Weber–Morris intraparticle diffusion model is expressed by the following equation:

$$q_t = K_i \cdot t^{0.5} + I, \tag{13}$$

where $I$ is the intercept related to the boundary layer effect and $K_i$ is the intraparticle diffusion rate constant which can be evaluated from the slope of the linear plots of $q_t$ versus $t^{0.5}$. If Weber–Morris plot of $q_t$ versus $t^{0.5}$ is linear and passes through the origin, the intraparticle diffusion is the sole rate-determining step, but when the plots in the figure are multilinear with three distinct regions; in that case, there are three different kinetic mechanisms. The initial region corresponds to the external surface uptake; the second stage

Table 3: The isotherm model constants and regression coefficient.

| $T$ (K) | Langmuir isotherm model | | | Error function | | Freundlich isotherm model | | | Error function | |
|---|---|---|---|---|---|---|---|---|---|---|
| | $Q^\circ$ | $b$ | $R^2$ | $\chi^2$ | RMSE | $K_F$ | $1/n$ | $R^2$ | $\chi^2$ | RMSE |
| 298 | 161.29 | 0.2059 | 0.998 | 0.969 | 4.96 | 52.07 | 0.2147 | 0.878 | 11.87 | 14.67 |
| 308 | 166.66 | 0.2255 | 0.997 | 0.913 | 4.73 | 52.35 | 0.2234 | 0.917 | 9.71 | 13.96 |
| 318 | 312.50 | 0.3950 | 0.998 | 0.851 | 0.964 | 85.11 | 0.3194 | 0.917 | 9.11 | 13.97 |
| 328 | 277.78 | 0.1791 | 0.998 | 4.21 | 12.79 | 59.08 | 0.3315 | 0.929 | 27.53 | 31.26 |

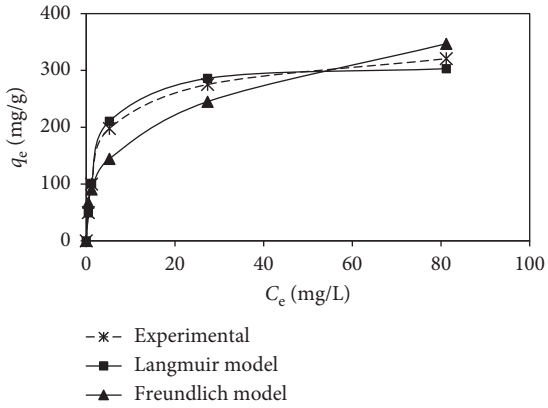


Figure 13: Comparison of the experimental and predicted isotherms for Cr(VI) adsorption (temperature 45°C and initial pH 3).

Table 4: Comparison of results obtained in this study for the adsorption of Cr(VI) with those of other adsorbents.

| Adsorbent | pH | Langmuir isotherm model | | References |
|---|---|---|---|---|
| | | $Q^\circ$ (mg/g) | $b$ (L/mg) | |
| Multiwalled carbon nanotubes | 4.28 | 1.177 | 0.526 | [27] |
| Commercial hematite [$\alpha$-$Fe_2O_3$] | 8 | 2.299 | 0.388 | [4] |
| Commercial activated carbon-Fe | 2.0–3.0 | 1.680 | 1.21 | [28] |
| Olive oil factory wastes | 2.0 | 18.69 | 0.0554 | [5] |
| Hydrous titanium(IV) oxide (CHTO) | 1.5 | 27.11 | 0.2766 | [29] |
| Activated carbon from rubber wood | 2.0 | 65.78 | 0.2443 | [24] |
| Graphene hybridized $Fe_3O_4$ nanoparticles | — | 78.50 | 0.0006 | [26] |
| *L. speciosa* bark embedded magnetic iron oxide nanoparticles | 2.05 | 434.78 | 11.499 | [1] |
| FeNPs synthesized with aqueous *E. japonica* leaves extract | 3.0 | 312.50 | 0.3950 | This study |

Table 5: Kinetic model parameters with regression coefficients and error functions for the pseudo-first-order kinetic model.

| $C_0$ (mg/L) | $q_{e,exp}$ (mg/g) | Pseudo-first-order | | | Error function | |
|---|---|---|---|---|---|---|
| | | $k_1$ (min$^{-1}$) | $q_{e,cal_1}$ (mg/g) | $R^2$ | $\chi^2$ | RMSE |
| 50 | 49.761 | 0.004145 | 5.237 | 0.431 | 39.84 | 44.52 |
| 100 | 100.95 | 0.011740 | 19.74 | 0.723 | 65.33 | 81.21 |
| 200 | 202.38 | 0.004600 | 119.92 | 0.748 | 33.60 | 82.46 |
| 300 | 297.85 | 0.004600 | 224.03 | 0.637 | 18.30 | 73.83 |
| 400 | 376.19 | 0.003915 | 361.83 | 0.799 | 0.55 | 14.36 |
| 500 | 458.81 | 0.003685 | 445.04 | 0.830 | 0.41 | 13.77 |

relates the gradual uptake indicating intraparticle diffusion as the rate-limiting step and final plateau region represents equilibrium uptake [31].

Based on the results, it was observed a multilinear plot (figure not shown) indicated that both intraparticle and film diffusion were effective on the adsorption of Cr(VI) on FeNPs. Moreover, according to Table 7, it was seen that the internal ($K_i$) and external diffusion constants ($I$) gradually increased with the increasing initial Cr(VI) concentration.

## 4. Conclusions

In summary, iron nanoparticles were biosynthesized by using a green, reducing agent, loquat leaves aqueous extract,

Table 6: Kinetic model parameters with regression coefficients and error functions for the pseudo-second-order kinetic model.

| $C_0$ (mg/L) | $q_{e,exp}$ (mg/g) | Pseudo-second-order | | | Error function | |
|---|---|---|---|---|---|---|
| | | $k_2$ (g/mg.min) | $q_{e,cal_2}$ (mg/g) | $R^2$ | $\chi^2$ | RMSE |
| 50 | 49.761 | 0.009040 | 50.237 | 0.999 | 0.0 | 0.48 |
| 100 | 100.95 | 0.003780 | 101.19 | 0.999 | 0.0 | 0.24 |
| 200 | 202.38 | 0.000535 | 199.27 | 0.994 | 0.05 | 3.11 |
| 300 | 297.85 | 0.000879 | 302.62 | 0.996 | 0.08 | 4.76 |
| 400 | 376.19 | 0.001181 | 401.90 | 0.997 | 1.76 | 25.71 |
| 500 | 458.81 | 0.000629 | 496.94 | 0.991 | 3.17 | 38.14 |

Table 7: Intraparticle mass transfer model parameters with regression coefficients.

| | Weber–Morris model | | |
|---|---|---|---|
| $C_0$ (mg/L) | $K_i$ (mg/g·min$^{0.5}$) | $I$ | $R^2$ |
| 50 | 0.3708 | 44.837 | 0.995 |
| 100 | 4.1859 | 70.642 | 0.995 |
| 200 | 5.2275 | 84.077 | 0.991 |
| 300 | 5.8675 | 107.30 | 0.998 |
| 400 | 5.9466 | 107.34 | 0.992 |
| 500 | 7.8679 | 108.88 | 0.996 |

and prepared FeNPs were tested as an adsorbent for Cr(VI) removal under our experimental conditions. The conclusions of this study can be summarized:

(i) The characterization studies confirmed the synthesis of FeNPs successfully. The synthesized FeNPs had irregular spherical morphology, and they were relatively agglomerated. The XRD spectrum showed the diffraction peaks belong to mainly iron hydroxide and iron oxyhydroxide. According to FT-IR spectrums, the peaks refer to Fe-O stretches of $Fe_3O_4$ and $Fe_2O_3$.

(ii) The optimum adsorption conditions were determined as initial pH 3.0, temperature 45°C, and adsorbent concentration 1.0 g/L. The uptake values at equilibrium increased linearly with the increasing the initial Cr(VI) concentration.

(iii) The adsorption equilibrium data were best fitted to the Langmuir isotherm model. The monolayer coverage capacity calculated from the Langmuir isotherm model was found to be 312.5 mg/g.

(iv) The thermodynamic parameters $\Delta G$, $\Delta H$, and $\Delta S$ were calculated as positive, and results indicated that the studied adsorption process was nonspontaneous, endothermic, and increasing in the randomness of adsorbed species.

(v) The adsorption kinetic data followed the pseudo-second-order kinetic model, and both intraparticle and film diffusion were effective on the adsorption process.

(vi) Based on the results, the biosynthesis method could be suggested for preparing iron nanoparticles in terms of eco-friendly, cost-effective, and easy-to-handle synthesis process with large scale, through the abundance of loquat or other plant leaves.

(vii) Consequently, green-synthesized FeNPs can be a good candidate for Cr(VI) removal owing to their high adsorption capacity.

## Nomenclature

$b$: A constant related to the affinity of the binding sites (L/mg)
$C_e$: Unadsorbed Cr(VI) metal ion concentration at equilibrium (mg/L)
$C_0$: Initial Cr(VI) metal ion concentration (mg/L)
$K_F$: Freundlich constant indicating adsorption capacity ((mg/g)/(L/mg)$^{1/n}$)
$K_i$: Intraparticle diffusion rate constant (mg/g·min$^{0.5}$)
$k_1$: Pseudo-first-order kinetic rate constant (1/min)
$k_2$: Pseudo-second-order kinetic rate constant (g/mg·min)
$q_e$: Adsorbed amount per unit mass of adsorbent (mg/g)
$q_{e,cal_1}$: Calculated adsorbed amount per unit mass of adsorbent from pseudo-first-order kinetic model (mg/g)
$q_{e,cal_2}$: Calculated adsorbed amount per unit mass of adsorbent from pseudo-second-order kinetic model (mg/g)
$q_{e,exp}$: Experimental adsorbed amount per unit mass of adsorbent (mg/g)
$q_t$: Adsorbed amount per unit mass of adsorbent at any time (mg/g)
$Q_o$: Maximum monolayer coverage capacity of adsorbent (mg/g)
$1/n$: Freundlich constant indicating adsorption intensity.

## Data Availability

The data used to support the findings of this study are available from the corresponding author upon request.

## Conflicts of Interest

The authors declare that they have no conflicts of interest.

## References

[1] S. Srivastava, S. B. Agrawal, and M. K. Mondal, "Synthesis, characterization and application of Lagerstroemia speciosa embedded magnetic nanoparticle for Cr(VI) adsorption from aqueous solution," *Journal of Environmental Sciences*, vol. 55, pp. 283–293, 2017.

[2] L. P. Lingamdinne, J. R. Koduru, Y.-L. Choi, Y.-Y. Chang, and J.-K. Yang, "Studies on removal of Pb(II) and Cr(III) using graphene oxide based inverse spinel nickel ferrite nanocomposite as sorbent," *Hydrometallurgy*, vol. 165, pp. 64–72, 2016.

[3] S. Abhalaxmi and S. K. Sahoo, "Magnetic nanoparticles: a novel platform for cancer theranostics," *Drug Discovery Today*, vol. 19, no. 4, pp. 474–481, 2014.

[4] O. Ajouyed, C. Hurel, M. Ammari, L. B. Allal, and N. Marmier, "Sorption of Cr(VI) onto natural iron and aluminum (oxy) hydroxides: effects of pH, ionic strength and initial concentration," *Journal of Hazardous Materials*, vol. 174, no. 1–3, pp. 616–622, 2010.

[5] E. Malkoc, Y. Nuhoglu, and M. Dundar, "Adsorption of chromium(VI) on pomace-An olive oil industry waste: batch and column studies," *Journal of Hazardous Materials*, vol. 138, no. 1, pp. 142–151, 2006.

[6] S. S. Baral, S. N. Das, and P. Rath, "Hexavalent chromium removal from aqueous solution by adsorption on treated sawdust," *Biochemical Engineering Journal*, vol. 31, no. 3, pp. 216–222, 2006.

[7] H. C. Vu, A. D. Dwivedi, T. T. Le, S.-H. Seo, E.-J. Kim, and Y.-S. Chang, "Magnetite graphene oxide encapsulated in alginate beads for enhanced adsorption of Cr(VI) and As(V) from aqueous solutions: role of crosslinking metal cations in pH control," *Chemical Engineering Journal*, vol. 307, pp. 220–229, 2017.

[8] S. Uysal, A. Cvetanović, G. Zengin, S. Đurović, and A. Aktumsek, "Optimization of the extraction process of antioxidants from loquat leaves using response surface methodology," *Journal of Food Processing and Preservation*, vol. 41, no. 5, article e13185, 2017.

[9] Y. Hong, B. Lin, H. Cao, Y. Gao, and S. Lin, "Analysis of major triterpene acids and total polysaccharides in the leaves of 11 species of eriobotrya," *BIO Web of Conferences*, vol. 8, article 03012, 2017.

[10] A. M. Awwad, N. M. Salem, and A. O. Abdeen, "Biosynthesis of silver nanoparticles using Loquat leaf extract and its antibacterial activity," *Advanced Materials Letters*, vol. 4, no. 5, pp. 338–342, 2013.

[11] A. Sharma, N. Dhiman, B. P. Singh, and A. K. Gathania, "Green synthesis of gold nanoparticles using extracts of *Artocarpus lakoocha* fruit and its leaves, andEriobotrya Japonicaleaves," *Materials Research Express*, vol. 1, no. 2, article 025042, 2014.

[12] M. Fazlzadeh, K. Rahmani, A. Zarei, H. Abdoallahzadeh, F. Nasiri, and R. Khosravi, "A novel green synthesis of zero valent iron nanoparticles (NZVI) using three plant extracts and their efficient application for removal of Cr(VI) from aqueous solutions," *Advanced Powder Technology*, vol. 28, no. 1, pp. 122–130, 2017.

[13] S. Kuo and R. Bembenek, "Sorption and desorption of chromate by wood shavings impregnated with iron or aluminum oxide," *Bioresource Technology*, vol. 99, no. 13, pp. 5617–5625, 2008.

[14] W. Liu, J. Zhang, C. Zhang, Y. Wang, and Y. Li, "Adsorptive removal of Cr(VI) by Fe-modified activated carbon prepared from *Trapa natans* husk," *Chemical Engineering Journal*, vol. 162, no. 2, pp. 677–684, 2010.

[15] T. Shahwan, S. Abu Sirriah, M. Nairat et al., "Green synthesis of iron nanoparticles and their application as a Fenton-like catalyst for the degradation of aqueous cationic and anionic dyes," *Chemical Engineering Journal*, vol. 172, no. 1, pp. 258–266, 2011.

[16] APHA, *Standard Methods for the Examination of Water and Wastewater*, American Public Health Association, Washington, DC, USA, 16th edition, 1981.

[17] A. Heller, M. S. H. Fleys, J. Chen, G. P. van der Laan, M. H. Rausch, and A. P. Fröba, "Thermal and mutual diffusivity of binary mixtures of n-dodecane and n-tetracontane with carbon monoxide, hydrogen, and water from dynamic Light scattering (DLS)," *Journal of Chemical & Engineering Data*, vol. 61, no. 3, pp. 1333–1340, 2016.

[18] Y. Kuang, Q. Wang, Z. Chen, M. Megharaj, and R. Naidu, "Heterogeneous Fenton-like oxidation of monochlorobenzene using green synthesis of iron nanoparticles," *Journal of Colloid and Interface Science*, vol. 410, pp. 67–73, 2013.

[19] A. M. Awwad and N. M. Salem, "Kinetics and thermodynamics of Cd(II) biosorption onto loquat (*Eriobotrya japonica*) leaves," *Journal of Saudi Chemical Society*, vol. 18, no. 5, pp. 486–493, 2014.

[20] T. Wang, X. Jin, Z. Chen, M. Megharaj, and R. Naidu, "Green synthesis of Fe nanoparticles using eucalyptus leaf extracts for treatment of eutrophic wastewater," *Science of the Total Environment*, vol. 466-467, pp. 210–213, 2014.

[21] R. K. Gautam, V. Rawat, S. Banerjee et al., "Synthesis of bimetallic Fe-Zn nanoparticles and its application towards adsorptive removal of carcinogenic dye malachite green and Congo red in water," *Journal of Molecular Liquids*, vol. 212, pp. 227–236, 2015.

[22] F. Hussain, S. Guo, and G. Zhang, "Preparation and characterization of bifunctional Ti–Fe kaolinite composite for Cr(VI) removal," *Journal of Colloid and Interface Science*, vol. 442, pp. 30–38, 2015.

[23] C.-H. Weng, Y. C. Sharma, and S.-H. Chu, "Adsorption of Cr(VI) from aqueous solutions by spent activated clay," *Journal of Hazardous Materials*, vol. 155, no. 1-2, pp. 65–75, 2008.

[24] T. Karthikeyan, S. Rajgopal, and L. Miranda, "Chromium(VI) adsorption from aqueous solution by sawdust activated carbon," *Journal of Hazardous Materials*, vol. 124, no. 1–3, pp. 192–199, 2005.

[25] N. C. Olivares, M. C. Díaz-Nava, and M. Solache-Ríos, "Enhanced decolorization of dyes by an iron modified clay and thermodynamic parameters," *Water Science and Technology*, vol. 73, no. 8, pp. 2007–2016, 2016.

[26] H. Gao, S. Lv, J. Dou et al., "The efficient adsorption removal of Cr(vi) by using $Fe_3O_4$ nanoparticles hybridized with carbonaceous materials," *RSC Advances*, vol. 5, no. 74, pp. 60033–60040, 2015.

[27] J. Hu, C. Chen, X. Zhu, and X. Wang, "Removal of chromium from aqueous solution by using oxidized multiwalled carbon nanotubes," *Journal of Hazardous Materials*, vol. 162, no. 2-3, pp. 1542–1550, 2009.

[28] P. Maneechakr and S. Karnjanakom, "Adsorption behaviour of Fe(II) and Cr(VI) on activated carbon: surface chemistry, isotherm, kinetic and thermodynamic studies," *Journal of Chemical Thermodynamics*, vol. 106, pp. 104–112, 2017.

[29] S. Debnath and U. C. Ghosh, "Kinetics, isotherm and thermodynamics for Cr(III) and Cr(VI) adsorption from aqueous solutions by crystalline hydrous titanium oxide," *The Journal of Chemical Thermodynamics*, vol. 40, no. 1, pp. 67–77, 2008.

[30] Y. Yan, Q. An, Z. Xiao, W. Zheng, and S. Zhai, "Flexible core-shell/bead-like alginate@PEI with exceptional adsorption capacity, recycling performance toward batch and column

sorption of Cr(VI)," *Chemical Engineering Journal*, vol. 313, pp. 475–486, 2017.

[31] S. R. Popuri, Y. Vijaya, V. M. Boddu, and K. Abburi, "Adsorptive removal of copper and nickel ions from water using chitosan coated PVC beads," *Bioresource Technology*, vol. 100, no. 1, pp. 194–199, 2009.